Analysis of diffusion in curved surfaces and its application to tubular membranes

Colin James Stockdale Klaus[a,†], Krishnan Raghunathan[b,†], Emmanuele DiBenedetto[a,b,*], and Anne K. Kenworthy[b,c,*]

[a]Department of Mathematics and [b]Department of Molecular Physiology and Biophysics, Vanderbilt University, Nashville, TN 37232; [c]Department of Cell and Developmental Biology, Vanderbilt University School of Medicine, Nashville, TN 37232

ABSTRACT **Diffusion of particles in curved surfaces is inherently complex compared with diffusion in a flat membrane, owing to the nonplanarity of the surface. The consequence of such nonplanar geometry on diffusion is poorly understood but is highly relevant in the case of cell membranes, which often adopt complex geometries. To address this question, we developed a new finite element approach to model diffusion on curved membrane surfaces based on solutions to Fick's law of diffusion and used this to study the effects of geometry on the entry of surface-bound particles into tubules by diffusion. We show that variations in tubule radius and length can distinctly alter diffusion gradients in tubules over biologically relevant timescales. In addition, we show that tubular structures tend to retain concentration gradients for a longer time compared with a comparable flat surface. These findings indicate that sorting of particles along the surfaces of tubules can arise simply as a geometric consequence of the curvature without any specific contribution from the membrane environment. Our studies provide a framework for modeling diffusion in curved surfaces and suggest that biological regulation can emerge purely from membrane geometry.**

Monitoring Editor
Patricía Bassereau
Institut Curie

Received: Jun 23, 2016
Revised: Sep 8, 2016
Accepted: Oct 4, 2016

INTRODUCTION

Lateral diffusion of proteins in membranes is ubiquitous and is known to play important roles in several cellular processes, including neuronal signaling, immunological reactions, receptor endocytosis, and many signaling pathways (Choquet and Triller, 2003; Douglass and Vale, 2005; Kusumi *et al.*, 2005; Eisenberg *et al.*, 2006; Lajoie *et al.*, 2007; Treanor *et al.*, 2010) The diffusion of biomolecules in membranes is actively modulated in cells through several mechanisms, including actin barriers and active fluctuations (Treanor *et al.*, 2010; Suetsugu and Gautreau, 2012; Jaumouillé *et al.*, 2014; Krapf, 2015; Trimble and Grinstein, 2015; Köster and Mayor, 2016). Diffusion of proteins in membranes is also sensitive to a number of factors, including the size of the protein, its confinement to domains, the viscosity of the environment, and crowding (Petrov and Schwille, 2008; Eggeling *et al.*, 2009; Kusumi *et al.*, 2010; Harb *et al.*, 2012; Edwald *et al.*, 2014). Classical studies on diffusion in cell membranes assume the surface to be planar and model diffusion in two dimensions (Saffman *et al.*, 1975). This assumption, though valid in studying many phenomena, may not be correct in studying diffusion in membrane deformations (Sbalzarini *et al.*, 2005; Leitenberger *et al.*, 2008; Adler *et al.*, 2010).

Manifestations of curvature in membrane are ubiquitous and have observable biological functionality. For instance, curvature is highly regulated in development and retraction of outgrowths in neurons (Guerrier *et al.*, 2009). Many processes such as recruitment of proteins, changes in composition of lipids, and changes in membrane physical properties are curvature dependent (Baumgart *et al.*, 2003; Carlton *et al.*, 2004; Roux *et al.*, 2005; Tian and Baumgart, 2009; Henle and Levine, 2010; Wu and Liang, 2014; Larsen *et al.*, 2015). Geometry is also known to play an important role in sorting of proteins. It has been hypothesized that the curvature of the *trans*-Golgi network (TGN) aids in protein sorting (Carlton *et al.*, 2004).

This article was published online ahead of print in MBoC in Press (http://www.molbiolcell.org/cgi/doi/10.1091/mbc.E16-06-0445) on October 12, 2016.

†These authors contributed equally to the manuscript.

C.J.S.K., K.R., E.D., and A.K.K. designed the research; C.J.S.K. and E.D. contributed new mathematical tools; C.J.S.K. and K.R. performed research; C.J.S.K., K.R., E.D., and A.K.K. analyzed data; C.J.S.K., K.R., E.D., and A.K.K. wrote the paper.

*Address correspondence to Anne K. Kenworthy (anne.kenworthy@vanderbilt.edu) and Emmanuele DiBenedetto (em.diben@vanderbilt.edu).

Abbreviations used: β2AR, β2 adrenergic receptor; FEM, finite element methods; FRAP, fluorescence recovery after photobleaching; TGN, *trans*-Golgi network.

Interestingly, the relative concentration of proteins and lipids in the membrane and tubules emanating from the membranes are different (Mukherjee and Maxfield, 2000, 2004; Roux *et al.*, 2005). This implies that molecular concentration in tubules and in the planar surface that they are connected to can be different, and this difference can have biological significance. Several researchers have elegantly shown that this sorting could arise through a variety of physical and biological mechanisms (reviewed in Callan-Jones *et al.*, 2011).

As with most physical properties of biological systems, curvature and shape of various membranes and membrane-bound organelles are highly regulated (Zimmerberg and Kozlov, 2006; Kozlov *et al.*, 2014; McMahon and Boucrot, 2015). In several cases, cells expend energy to maintain the geometry of these structures, as illustrated by recruitment of BAR domain proteins to sites of endocytosis (Rao and Haucke, 2011). Because geometry is tightly regulated in a cell, it is possible for the cells to modulate geometry to steer diffusion and concentration gradients. An important factor responsible for this, although less understood, is how biomolecules diffuse differently simply as a result of the nonplanarity of the surface (Yoshigaki, 2007; Kusters *et al.*, 2013). This influence of geometry on diffusion has been demonstrated for tubular geometries. Experimentally determined diffusion constants measured for a protein KvAP have been shown to be directly proportional to the radius of the tubule in which the protein diffuses (Domanov *et al.*, 2011; Aimon *et al.*, 2014). However, even the measurement of diffusion coefficients in nonplanar geometries could be inherently difficult due to the complexity of geometry (Sbalzarini *et al.*, 2005; Daniels and Turner, 2007; Domanov *et al.*, 2011; Renner *et al.*, 2011). Thus there is a real need to develop models that accurately measure the diffusion of molecules in complex geometries.

In this paper, we examine how the geometry of a surface plays a role in diffusion of molecules and, consequently, how concentration gradients of diffusing species develop. To address this, we developed a numerical implementation of the Laplace–Beltrami mathematical model to understand diffusion in geometrically complex surfaces using membrane tubules as a biologically relevant example. Tubular membrane geometries are typical of many structures found in cells, including dendritic spines, the endoplasmic reticulum, membrane nanotubes, primary cilia, clathrin-independent carriers, and sorting tubules emanating from endosomes and the TGN (Waterman-Storer and Salmon, 1998; Sorra and Harris, 2000; Pazour and Witman, 2002; Carlton *et al.*, 2004; Upadhyaya and Sheetz, 2004; Römer *et al.*, 2007; Domanov *et al.*, 2011; Day *et al.*, 2015). We report numerical simulations of the mathematical model that incorporate the cylindrical nature of tubules and the effect of the cylindrical geometry on diffusion of molecules along the tubule surface. We show by adapting standard diffusion paradigms that geometry has a nontrivial influence on diffusion and thereby the concentration of molecules that diffuse into tubules. These mathematical considerations predict that nonplanarity of membranes prolongs concentration gradients across a tubular surface. The amplitude and temporal spread of the concentration gradient is systematically dependent on the curvature of the tubule and the diffusion coefficient of the molecule. Thus our results imply that biological regulation can emerge from a strategic coupling of these geometric constraints with the cellular sorting machinery.

RESULTS

Diffusion in membranes has been characterized by a wide variety of theoretical techniques, including some that describe a tubular geometry (Saffman *et al.*, 1975; Berk and Hochmuth, 1992; Yoshigaki, 2007; Kusters *et al.*, 2013). Many of these methods use random-walk simulations, which apply stochastic models to describe diffusion. While these methods have been highly successful in addressing many interesting biological questions, they only asymptotically solve the diffusion equation of inherent interest and so add an extra order of approximation. Therefore, to understand how diffusion scales with different geometric parameters on a tubular surface, we described classical motion of diffusion set on a surface. We then derived a Laplace–Beltrami operator for the diffusion equation and solved it using finite element methods (FEM) for a symmetric condition (Supplemental Text S1). See also Supplemental Text S2 for the more general case of nonsymmetric conditions.

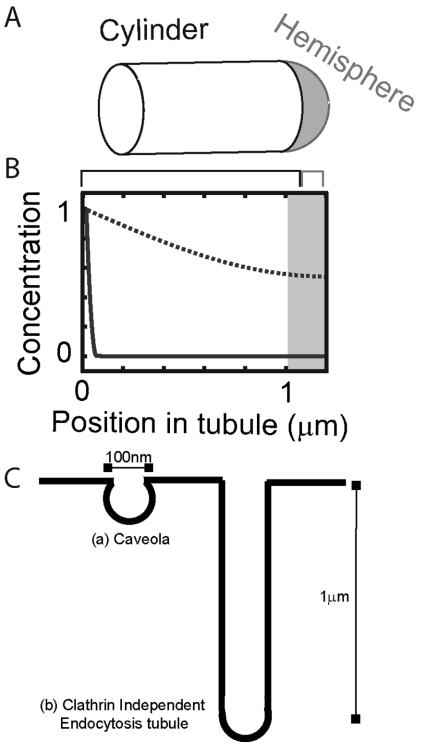

FIGURE 1: Representation of concentration along tubular surface. (A) A tubule is described as two geometric structures: a cylindrical portion (clear) and a hemispherical portion (gray). (B) Example of plots of concentration of diffusing species for a tubule with length 1 μm and radius 200 nm. The shaded portion corresponds to the hemisphere region, and the white portion represents the cylindrical region of the tubules. The dotted and solid lines illustrate two different arbitrary concentration profiles. (C) Illustration of the difference in length scales of membrane tubules in biology.

We solved the Laplace–Beltrami equations to understand how various geometric parameters affect diffusion and thereby the concentration gradient of a diffusing species along the surface of a tubule for a prescribed boundary condition. A tubule is modeled as a cylinder with length *h* and radius *r* attached to a hemispherical cap of radius *r*. A cartoon representation of a tubule is shown in Figure 1A. We considered a range of radii and lengths that mimic various dimensions of membrane tubules found in cells or generated in vitro (Table 1 and Figure 1C). The geometry of the tubule is assumed to be constant as a function of time. This implies that molecules diffuse into pre-existing tubules. Such tubules are common in biological systems. Unless otherwise specified, we assume that diffusing species enter the tubule from the open rim and diffuse into the body of the tubule. We want to emphasize that all diffusion conditions described in this paper refer solely to surface diffusion along

Structure	Radius (nm)	Height	Reference
Clathrin-coated pits	Pits 20–80 Coats 35–100		Kirchhausen, 2009
Caveolae	40–60	100 nm	Westermann *et al.*, 1999
Cholera toxin endocytic tubules	≤250	5 μm	Day *et al.*, 2015
Shiga toxin endocytic tubules	≤250	1–20 μm	Römer *et al.*, 2007; Renard *et al.*, 2015
Filopodia	100	1–2 μm	Mogilner and Rubinstein, 2005
PACSIN2 tubes	10–100		Wang *et al.*, 2009
Endophilin A2 tubules	10–50		Farsad, 2001
Endoplasmic reticulum tubule	57		Upadhyaya and Sheetz, 2004
Golgi tubule	90		Upadhyaya and Sheetz, 2004
Inner mitochondrial tubule	18		Scorrano *et al.*, 2002
Neurites	25–1250	≥1μm	Windebank *et al.*, 1985; Briggman and Bock, 2012

TABLE 1: Examples of length and radii of membrane tubules.

tubules and not diffusion in the lumen of the tubule. A reservoir of molecules is assumed to be present outside the rim and available to diffuse into the tubule. Diffusion from the rim into the tubule occurs with a defined diffusion coefficient *k*, which falls within a range of values previously reported for membrane-associated proteins (Daumas *et al.*, 2003; Kenworthy *et al.*, 2004). Note that the model only considers the effects of geometric factors on diffusion. Thus the diffusing species have no explicit size or shape, the surface of the tubule does not have a defined thickness, and the regions inside or outside the tubule have no viscosity. Correspondingly, hydrodynamic effects are not included in this model.

To understand how material diffuses on the tubules as a function of time, we typically generate plots of the concentration of diffusing species along the length of the tubule, where the rim of the tubule is set as 0. Note that the coordinate system used in the figures is different from the coordinate system used while solving the Laplace–Beltrami equation. An explanation and the relationship between the coordinate system used in the figure and in the equation are described in Supplemental Text S3 and in Supplemental Figure 2. Examples of two possible concentration gradients are illustrated in Figure 1B. For these cases, the concentration of diffusing species is identical at the rim but differs along the length of the tubule.

How does geometry impact the time it takes for material to equilibrate along the surface of a tubule?

In subsequent sections, we simulate biologically relevant tubular dimensions and boundary conditions to understand how molecules in tubules diffuse. We expect the geometry of the tubule to control the diffusion of molecules along its surface in two ways. First, geometry should regulate the time it takes for a molecule to equilibrate completely across the length of the tubule. Second, geometry can influence how concentration scales spatially along the length of the tubule. We performed simulations to understand the magnitude of each of these effects. To carry out these studies, we considered tubule lengths and radii similar to those seen in biological membranes (Table 1 and Figure 1C). Diffusion coefficients ranging from 0.01 to 0.5 $\mu m^2/s$ were chosen to mimic those previously reported for membrane proteins (Daumas *et al.*, 2003; Kenworthy *et al.*, 2004).

To investigate the impact of tubule geometry on the equilibration time, we simulated a condition in which the concentration of diffusing species within the surface of the tube is initially 0 except at the rim, where it is set as 1. We assume that the concentration of diffusing species available to enter the rim of the tube remains constant throughout the time course of the simulation. This boundary condition represents a unity Dirichlet data, and the simulations with this boundary condition are referred to subsequently as Dirichlet simulations purely for the sake of convenience. This represents a biological condition in which the surrounding membrane is saturated with molecules at all times. These molecules will then diffuse into the tubule until equilibrium is reached between the membrane and tubule.

We first characterized diffusion onto a tubule as a function of time under the Dirichlet boundary condition. For this, we selected a tubule with radius of 0.1 μm and length 1 μm and set the diffusion coefficient as 0.1 $\mu m^2/s$. We then simulated the concentration of diffusing material across the tubule surface at 0.25 s intervals for a total time of 10 s. Under these conditions, the magnitude of the concentration gradient across the tubule systematically decreases, and eventually the tubule fully equilibrates to a concentration of 1 (Figure 2A). Correspondingly, a plot of the average concentration of diffusing species in the tube saturates as a function of time (Figure 2B). From such plots, the half-time ($t_{1/2}$) required for equilibration can be directly calculated.

We next investigated how diffusion coefficient, tubule radius, and tubule length alter the equilibration time. For these studies, we varied each of the parameters individually, keeping the other two constant. First, we varied diffusion coefficients from 0.01 to 0.5 $\mu m^2/s$ on a tubule of length 1 μm and radius 0.1 μm for a total simulation time of 5 s. Not surprisingly, for faster diffusion coefficients (Supplemental Figure 3), the diffusing species equilibrates faster, while for slower diffusion coefficients, the equilibration is considerably slower. For example, diffusing species with a diffusion coefficient of 0.5 $\mu m^2/s$ have a half-time of ~0.5 s, whereas a 10-fold slower diffusion coefficient of 0.05 $\mu m^2/s$ yields a half-time of ~4.5 s.

Next we simulated diffusion on tubules of variable lengths, assuming a constant radius of 0.1 μm and a diffusion coefficient of 0.1 $\mu m^2/s$ (Supplemental Figure 4A). While the shortest tubule (h = 0.1 μm) equilibrated rapidly, as expected, even lengths of 0.5 μm posed a significant barrier to the diffusion of molecules onto the tubule (Supplemental Figure 4B). To generalize how the length of the tubule affects equilibration, we calculated the half-time ($t_{1/2}$) of the tubule to equilibrate (Figure 2C). For tubules that had not reached half-saturation by the end of the simulation, we used extrapolation to obtain $t_{1/2}$. We found that $t_{1/2}$ is not linear for small

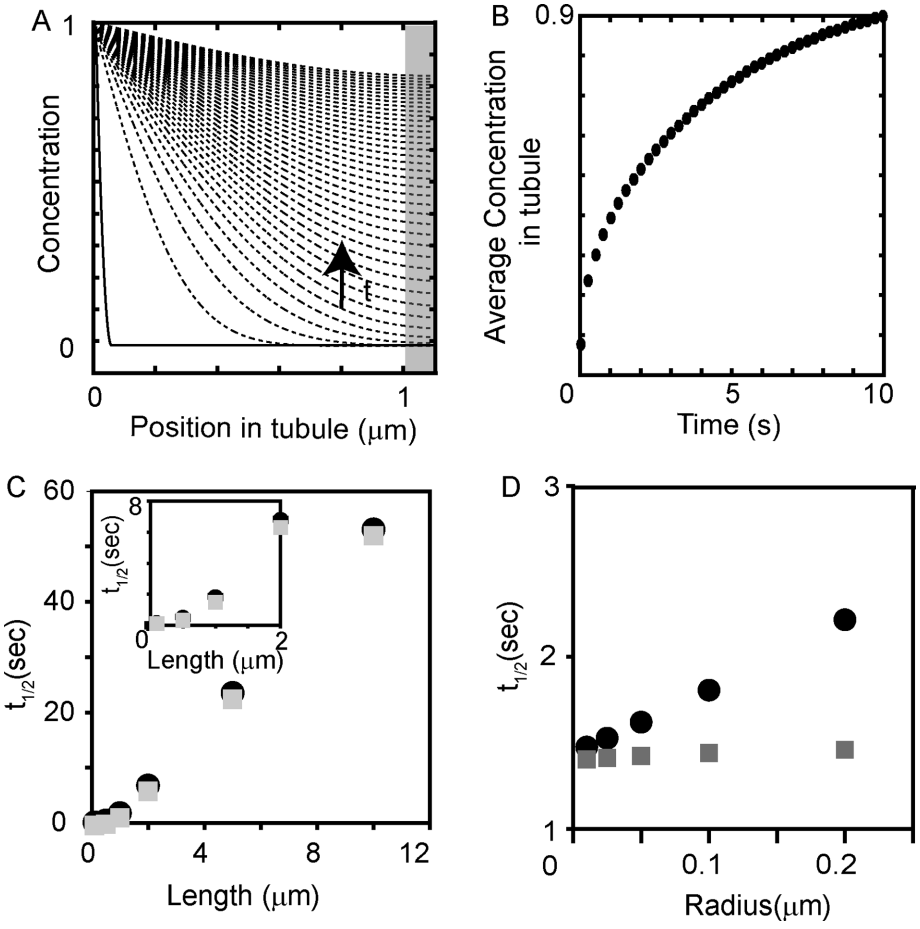

FIGURE 2: Variation of concentration along the tubule over time under Dirichlet boundary conditions. (A) Evolution of concentration gradients as a function of time for a Dirichlet simulation of molecules actively flowing into a tube of length 1 μm and radius 0.1 μm with a diffusion coefficient of 0.1 μm^2/s shown for time steps of 0.25 s. The zero time point is indicated by the solid line and the subsequent time points are shown as dashed lines. The arrow indicates increasing time. (B) Change in average concentration of molecules in the tubule as a function of time for the case of the unity boundary conditions. (C) Half-time ($t_{1/2}$) required to fully equilibrate material along the entire tubule (black circles) or the cylindrical region only (gray squares) as a function of tubule length for a tubule of radius 0.1 μm. Inset shows $t_{1/2}$ for small lengths. (D) $t_{1/2}$ required to fully equilibrate material across the entire tubule (black circles) and the cylindrical portion only (gray squares) as a function of tubule radius for a tubule with length of 1 μm.

lengths (Figure 2C, inset), but for lengths >2 μm, it increases linearly, since the contribution from the hemispherical region is negligible. We also determined the $t_{1/2}$ for the cylindrical portion only and found that this closely resembles the $t_{1/2}$ of the entire tube, especially for long tubules. When we attempted to do the same for the hemisphere, we found that, for longer length scales, the hemisphere was devoid of diffusers, and extrapolations were therefore not accurate. Thus these have not been reported here.

We next simulated diffusion in tubules with a constant length of 1 μm but radii ranging from 0.01 to 0.2 μm (Supplemental Figure 4D). These simulations were carried out for a time period of 5 s. As before, we determined the $t_{1/2}$ required for material to equilibrate along the entire tube or the cylindrical region (Figure 2D). The results of these simulations show that increasing the tubule radius from 0.01 to 0.2 μm slows down the entry of material onto the tubule. For example, the time it takes for the average tubule to become half-saturated increases from almost 1.5 to 2.2 s when the radius is increased from 0.01 to 0.2 μm, translating to almost a 50% increase.

How does geometry influence the magnitude of concentration gradients across the surface of the tubules?

In the scenario outlined above, we considered a situation in which the material that enters the tubules is present at constant levels in the membrane reservoir. However, under some conditions, the concentration of material available to enter the tubes may itself vary as a function of time, for example, as the result of a chemical reaction or signaling event. To model this situation, we considered a second boundary condition, in which we assumed that the concentration of diffusing species is initially 0 both across the surface of the tube and at the rim at $t = 0$. A linearly increasing quantity of molecules was then added to the rim as a function of time, and the molecules then diffused onto the tubule. Because the flow is unity and increasing, this boundary conditions represents a unity Neumann data, and the simulations are henceforth referred to as Neumann simulations for the sake of convenience. We then examined how concentration evolves as a function of time for the same tubule dimensions and diffusion coefficients simulated for the Dirichlet boundary condition.

We first characterized how a typical Neumann boundary condition evolves by using as an example a molecule with a diffusion coefficient 0.1 μm^2/s diffusing onto a tubule of radius 0.1 μm and length 1 μm. Figure 3A shows the concentration gradients along the length of the tubule as a function of time over 0.25 s time intervals (dashed lines) beginning at time $t = 0$ (solid line) for a total of 10 s. Unlike the Dirichlet boundary condition, here the concentration of material in the tubule grows without bounds as the result of the constant rate of influx of molecules at the rim for as long as that constant rate of influx is prescribed (Figure 3A). Consequently, for a given tubule, the overall shape of the gradient is maintained over time, and the total concentration rises linearly (Figure 3B). To provide a measure of the relative differences in concentration at the rim and the tip of the tubule at the end of these simulations, we define an "exclusion factor" term as exclusion factor $= (C_0 - C_1)/(C_0)$, where C_1 and C_0 are the concentration of molecules at the rim and the end of the tubule. This factor ranges from 0 to 1, with 1 implying that the tubule bottom has 0 concentration and 0 representing an equilibrated state with equivalent concentrations at the tubule rim and tip.

To study how tubule geometry influences the way molecules are sorted into tubules, we varied the length and radius of the tubule and the diffusion coefficient of the diffusing species to determine the corresponding concentration gradients. We would like to stress that, in real biological systems, this condition would not continue indefinitely and would have an upper bound on the time up to which material flows. Hence we compare the concentration profiles and "exclusion factor" (Supplemental Text S4) between different conditions at a single time point ($t = 5$ s) for the different Neumann

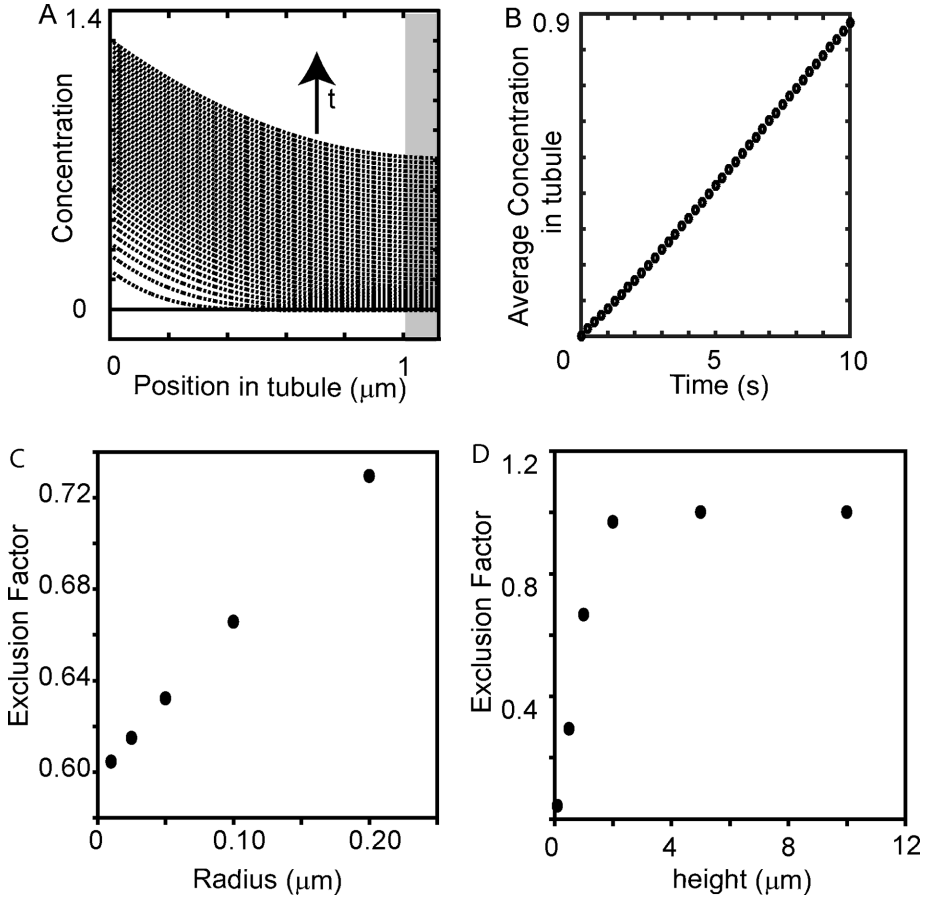

FIGURE 3: Variation of concentration along the tubule surface under Neumann boundary condition simulations. (A) Evolution of concentration gradients as a function of time for a Neumann simulation of molecules actively flowing into a tube of length 1 μm and radius 0.1 μm with a diffusion coefficient of 0.1 $\mu m^2/s$. The zero time point is indicated by the solid line and the subsequent time points are shown as dashed lines (time steps = 0.25 s). (B) Change in average concentration of molecules along the tubule surface as a function of time in the case of the unity Neumann boundary conditions. (C) Effect of changing the radius of a tubule on the exclusion factor for a molecule with diffusion coefficient of 0.1 $\mu m^2/s$ while keeping the length of the tubule constant at 1 μm. (D) Effect of changing the length of a tubule on the exclusion factor for a molecule with diffusion coefficient of 0.1 $\mu m^2/s$ while keeping the radius of the tubule constant at 0.1 μm.

simulations. This time point was chosen arbitrarily to emphasize diversity in concentration gradients for the different parameters we compared. The flow rate was likewise held constant across our simulations.

First, we investigated how diffusion coefficients impact the evolution of concentration gradients across the surface of a tubule of constant length 1 μm and radius 0.1 μm for a simulation time of 5 s. Not surprisingly, as shown in Supplemental Figures 5 and 6, increasing the diffusion coefficient increased the absolute concentration of material present within the tubule. Interestingly, increasing the diffusion coefficient also decreased the "exclusion factor" (Supplemental Text S4). Thus the less mobile a molecule is, the less its gradient relative to the reservoir.

Next we studied the effect of tubule radius (Supplemental Figure 7A) by simulating molecules diffusing into tubules of a constant length 1 μm and diffusion coefficient of 0.1 $\mu m^2/s$ for a period of 5 s. For this analysis, we kept the concentration of molecules available at the rim for diffusion as a constant, implying that the total number of molecules available differs as a function of radius. We found that changing the radius does not substantially impact the underlying characteristics of the concentration profile in the tubule, although we did note that at the largest radius, r = 0.2 μm, a concentration gradient was present at the bottom of the tube. This presumably reflects the fact that the radius is comparable to the tube length. As the tube radius was decreased, a higher density of molecules accumulated in the bottom of the tubule. This behavior is also reflected in the "exclusion factor" increasing linearly with increasing radii for this range of values (Figure 3C).

Finally, we varied the length of the cylindrical region to determine the effects of tube length. We varied the tubule length over two orders of magnitude ranging from 0.1 μm up to 10 μm with a constant tubule radius of 0.1 μm under the Neumann boundary condition. We observed that overall concentration gradients are different for different tubule lengths with identical radii (Supplemental Figure 7B). As seen from the "exclusion factor" (Figure 3D) for very small length scales, for instance for h = 0.1 μm, the length is sufficiently small for the entire tubule to be exposed to diffusing molecules within 5 s, resulting in a relatively uniform concentration across the entire tubule. The plateau seen in the exclusion factor occurs because material has not yet reached the hemispherical region and, hence, for these geometries at this time point, the exclusion factor would remain the same. In the case of long tubules, the hemisphere and even some portions of the cylindrical region are not even exposed to the diffusing molecules. However, length of the tubule, more than radius is a chief contributing factor in determining the exclusion factor.

Comparison of diffusion of molecules in a tubular surface and a flat surface

Until now, we have compared the diffusion of molecules along a tubular surface of various dimensions. To understand the importance of tubular geometry on diffusion from a more general perspective, it is useful to compare diffusion on a tubule to diffusion on a flat surface. Such a comparison requires one to define a geometrically comparable noncurved surface. However, due to Gaussian curvature obstructions, we cannot expect these systems to be pointwise comparable in the mathematical sense of isometric equivalence. A Riemannian isometry would erase the very local curvature differences we aim to explore. Instead, we design surfaces that are comparable by enforcing that they share a common amount of total *material* (area). By this, we preserve *global* area, and the same total area is available to diffusion in both systems, though in one it is shaped like a curved tube and in the other like a flat disk. In this sense, differences in diffusion are solely due to differences in curvature between the systems. We designed such a control by defining a planar disk containing an outer annulus with an area corresponding

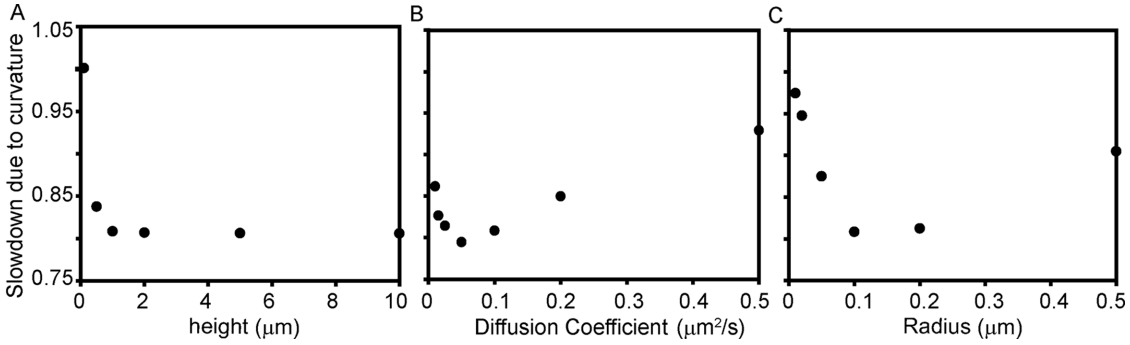

FIGURE 4: Comparison of concentration gradients in flat surfaces and in tubules. Slowdown of diffusion in the tubular geometry was quantified at the rim of the hemisphere–cylinder junction as slowdown $= (C_0 - C_{0.25})_{\text{tubule}} / (C_0 - C_{0.25})_{\text{flat}}$ between time $t = 0$ s and $t = 0.25$ s. (A) Effect of tubule length with tubule radius and diffusion coefficient held constant at 0.1 μm and 0.1 μm^2/s, respectively. (B) Effect of diffusion coefficient with tubule radius and length held constant at 0.1 and 1 μm, respectively. (C) Effect of tubule radius with tubule length and diffusion coefficient held constant at 1 μm and 0.1 μm^2/s, respectively.

to the cylindrical area of the tubule and an inner circular region with an area equal to the hemispherical region of the tubule (Supplemental Text S1 and Supplemental Figure 8). In this manner, the vertical tube and flat annulus respectively surround the hemisphere and corresponding disk in two and three dimensions. We then described the flat surface using the same coordinate system used to describe the tubules.

Using this equivalent geometric description, we simulated conditions to compare diffusion in curved tubes with that on comparable planar disks. To carry out these simulations, we used an initial condition in which the molecules were present uniformly in the hemispherical region or its corresponding planar region and allowed them to diffuse into the cylindrical region or its flattened equivalent for a total time of 5 s. Thus, unlike the previous simulations, where the material diffused from the open rim of the cylindrical region of the tubule, in these simulations material diffuses from rim of the hemisphere into the cylindrical region of the tube. The initial value of concentration was arbitrary set at 1000 U. In addition, these simulations have a closed boundary condition, in that the molecules do not flow out of the tube.

We performed the simulation with the initial boundary conditions described above, except that, in this case, the hemisphere contained a uniform concentration of diffusing species at $t = 0$. Thus, for these simulations, the concentration gradient should dissipate outward toward the tubule rim given sufficient time. However, comparison of the diffusion as a function of time between two distinct geometries could be extremely arbitrary. At the start of the simulation, the two conditions have similar concentration, and in many cases, both the tubule and the flat surfaces could be completely equilibrated at the end of the simulation. Hence it becomes important to compare them using a temporally equivalent parameter. Similarly, the difference between the two geometries could be spatial as well. Therefore, to compare the rate of dispersal of material between the two different geometries, we introduce a "slowdown" parameter, which incorporates both the spatial and temporal components as a single measure. This is calculated at the rim of the hemisphere–cylinder junction as slowdown $= (C_0 - C_{0.25})_{\text{tubule}} / (C_0 - C_{0.25})_{\text{flat}}$ between time $t = 0$ s and $t = 0.25$ s (the first time step in these simulations). The numerator terms, C_0 and $C_{0.25}$, denote the concentration at the junction of the two surfaces (cylinder and hemisphere) for the tubule for times $t = 0$ and 0.25 s, respectively, while the denominator denotes the concentration at the intersection of the two concentric annuli of the flat surface for the same two time steps. The "slowdown parameter" is in essence the ratio of how fast molecules can diffuse out of a tubular surface compared with a flat surface. By this measure, a value of 1 indicates the tubule and the flat geometry match. While this quantification of slowdown is arbitrary, it enables us to study the relative effects of flat versus tubular geometries on diffusion. The slowdown parameter is explained in detail in Supplemental Text S5.

As before, we varied the three parameters of interest (radius, length, and diffusion coefficient), but in this case, we carried out simulations for both flat and curved surfaces. In every case examined, we found that, compared with the flat geometry, the loss of material from the hemisphere was slowed in the tubular geometry (Figure 4). In some cases, the magnitude of this effect was nearly 20%. When we increased the length of the tubule, the effective slowdown due to tubular geometry reached an asymptotic value. This is because the effect of hemispherical region is minimal for lengths greater than 1 μm, and thus all longer tubules behave identically at the early time points. However, the effects of radii and diffusion coefficient were nonsymmetrical paraboloids, suggesting that a complex relationship exists between these parameters.

Comparison with experimental results

To assess the validity of our models, we compared our simulations with a recent experimental work by Aimon *et al.* (2014), who measured diffusion of proteins in membrane tethers connected to a giant unilamellar vesicle using a fluorescence recovery after photobleaching (FRAP) assay. In these experiments, an entire tubule of a defined length and radius was photobleached and allowed to recover (Figure 5). The diffusion coefficient was then determined using a theoretical solution for diffusion in the special case of a long, thin cylinder connected to a sphere that acts as a reservoir for the diffusing molecules (Berk and Hochmuth, 1992). Both experiments were performed on tubes with a length of 6 μm but slightly different radii of 30 and 20 nm and contained two different proteins whose diffusion coefficients were quantified as 0.73 and 0.38 μm^2/s.

To compare these experimental photobleaching data with our diffusion model, we simulated diffusion on these exact geometries using the experimentally determined diffusion coefficients. We assumed that, at time $t = 0$, the tubule contains no diffusing species except at the rim, which is attached to a reservoir with a uniform concentration of one. We simulated diffusion into the tubes for 80 s and then calculated the average concentration of diffusing species across the tubule surface over time. The data obtained

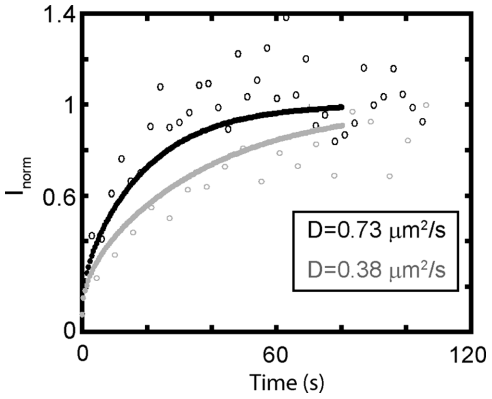

FIGURE 5: Comparison of simulated diffusion with previously published experimental data (Aimon *et al.*, 2014). The experimental recovery curve data are adapted from Figure 3 (gray circles) and Figure S3B (black circles) of Aimon *et al.* (Original data depicted in the figure as gray/black open circles and the diffusion coefficients were kindly provided by Patricia Bassereau, Institut Curie.) The open circles denote the original FRAP data from the paper, and the lines denote the recovery curve from the simulation, adapting the geometry and diffusion coefficients measured in the paper.

from the simulation closely agree with the data obtained experimentally (Figure 5). Thus our simulations capture this special geometric scenario, corroborating our approach using the finite element model for solving the Laplace–Beltrami equation.

DISCUSSION

Understanding how geometry influences diffusion of molecules on membrane surfaces has important cell biological implications. In this paper, we have developed a mathematical framework to describe how geometry influences diffusion using a tubular surface as a model system. This geometry occurs in a number of biologically important structures, including primary cilia, dendritic spines, endosomal tubules, and clathrin-independent endocytic carriers. For diffusion along the curved surface, the local area available for diffusion is different relative to a flat surface. This gives rise to a strong dependence of diffusion on the tubule geometry. We examined three key parameters that can potentially influence diffusion—the tube radius, the length of the tubule, and the diffusion coefficient of the diffusing species—using a range of biologically relevant values of these parameters. We found that each of these variables plays a distinct role in regulating diffusion, depending on the boundary conditions. We also compared diffusion in tubular structures with that in a comparable flat surface and showed that the tubular geometry slows down diffusion.

The model described in our paper represents a significantly different approach for understanding diffusion in surfaces with complex geometries compared with many other earlier models that typically use random-walk motion and escape times of molecules to determine geometric effects on diffusion (Yoshigaki, 2007; Jiang and Powers, 2008; Callan-Jones *et al.*, 2011; Holcman and Schuss, 2011; Singh *et al.*, 2012; Kusters and Storm, 2014; Kusters *et al.*, 2014). Our model represents a simple but fundamental formulation of a diffusion equation in a static tube. Compared with random-walk approaches, in which the only modeling degree of freedom is the random variable describing the walk of an individual particle (Gikhman and Skorokhod, 1969), a diffusion equation–based method requires less restrictive assumptions about individual particle motions. In our model, the dynamics at the boundary are prescribed and not merely observed, and the a priori knowledge of the boundary reconstructs the system behavior. An alternate approach to solving diffusion equations would be to use analytical approaches. This approach is typically not feasible for complex geometries and boundary conditions. In case of a tubule, for example, the adjoin of the hemisphere and tube disallows the use of analytical methods due to the need to "knit" the solutions across the boundary of the two geometries. To obtain a solution in the whole tubule (i.e., across the separating boundary), one has to ensure continuity of the solution and continuity of fluxes across such a boundary. Enforcing such conditions could result in at least one of the two problems (in their own regions) being overdetermined. Iteration techniques typically lead to issues of convergence, and the limit may not be expected to be explicit in some topologies. In this paper, we have sought to present a method that may be directly applied to many future real-world geometries of interest. In these cases, numerical methods will be the only realistic recourse for determining solutions. Further, to broaden the scope of usage of our model, we have implemented another parallel approach of solving the Laplace–Beltrami using virtual coordinates, and this has been described in Supplemental Text S2. Thus, compared with the "1-D" used in the simulation, this framework can model more general boundary conditions such as asymmetric initial boundary conditions (Supplemental Figure 1C), and the models presented here can be applied to any arbitrary surface geometry and boundary condition.

In this study, we focused on understanding how geometric effects impact concentration gradients under conditions that are relevant to tubular structures found in biological membranes. We acknowledge that this description is still incomplete, as other factors could potentially impact how concentration gradients evolve for a given tubule geometry and diffusion coefficient. The most prominent of these factors that are not included in the present model is the effect of hydrodynamics (Arroyo *et al.*, 2010; Rahimi and Arroyo, 2012; Rahimi *et al.*, 2013; Kosmalska *et al.*, 2015). Membranes can be approximated as a viscous fluid enclosed by fluids on both sides. Recent studies have shown that hydrodynamics vary as a function of tubule geometry for membranes (Daniels and Turner, 2007; Henle and Levine, 2010; Henle *et al.*, 2007; Domanov *et al.*, 2011), which in turn could alter the way molecules diffuse in tubules. Similarly, our model does not account for the size of the diffusing species, which could also be critical for understanding diffusion in a real membrane (Guigas and Weiss, 2006). Earlier experiments have shown that the protein and lipid composition of membrane tubes themselves can be curvature dependent, which could potentially introduce additional constraints on diffusion (Callan-Jones *et al.*, 2011; Aimon *et al.*, 2014). To delineate these factors from differences arising purely from geometry, we have included a program (Supplemental Text S6) that can determine the "expected diffusion coefficient" given $t_{1/2}$ (as measured in FRAP experiments) for concentration equilibration for a given tubule geometry. Comparison of diffusion coefficients obtained from the simulation with those obtained from other empirical models (Berk and Hochmuth, 1992) that incorporate factors such as hydrodynamic effects (Daniels and Turner, 2007) will decouple these two factors. In the case of long thin tubules, our simulated diffusion profile resembles but is not identical to the experimentally observed diffusion profiles (Aimon *et al.*, 2014), as demonstrated in Figure 5. In the two examples, we see that the difference in $t_{1/2}$ as predicted from our model is 20–30% different from the experimental values modeled using an empirical model for this particular case (Berk and Hochmuth, 1992). The discrepancy between the two values could potentially arise from hydrodynamic effects.

Even just using first principles and varying only relative geometry, we can make several interesting predictions about material flow and concentration gradients arising from diffusion in tubules with relevance to biological processes occurring in membranes. One such prediction is that diffusion of a particle in a tubular structure appears to be slower than its diffusion in a flat surface, simply as a consequence of geometric effects. This can be thought about as a loss of freedom due to the constrained geometry imposed by the curvature. Thus, while the total areas of the tubular and the flat surface are equal, the local area for the diffusion of molecules is reduced in a tubular geometry due to radial curvature, thus prolonging the gradient. This effect could potentially explain recent observations that diffusion of membrane proteins is slower in tubules than the surrounding "flat" membranes in vitro (Domanov *et al.*, 2011). The predicted slowdown also confirms other theoretical works by groups who have investigated diffusion in curved surfaces. For instance, Kusters and Storm (2014), using random-walk simulations of single particles diffusing on tubes, have shown that curved surfaces retain molecules for an increased period of time before the molecules escape. The predicted slowing down of diffusion due to curvature effects was shown to influence receptor egress from the dendritic spine (Kusters *et al.*, 2013). This is analogous to the retention of a concentration gradient along the tubule length due to its inherent curvature. Most models and experiments assume that the changes in diffusion with curvature are due to the altered diffusion coefficients of molecules (Berk and Hochmuth, 1992; Domanov *et al.*, 2011; Zhu *et al.*, 2012; Aimon *et al.*, 2014). However, from a fundamental standpoint, our results show that geometry itself can also contribute to such effects. This delineation between diffusion coefficient changes and geometric slowdown is a critical, yet underrealized aspect of diffusion that readily emerges from our work.

Our model also predicts a priori the conditions that would increase the entry or retention rate of molecules in tubules. Because the tubular nature of the membrane stretches out the concentration gradient temporally, it leads to an interesting hypothesis, that is, cells can tune the geometry of tubes as a mechanism to regulate the entry and exit of membrane-associated cargo. Modulation of concentration gradients could potentially be one reason why curvature in membrane tubules is tightly regulated by proteins such as BAR domain proteins (Rao and Haucke, 2011; Ramesh *et al.*, 2013; Simunovic *et al.*, 2015). Of the three parameters we examined (tubule height, tubule radius, and diffusion coefficient), within the limits of biological molecules, we found that tubule height was a key parameter affecting the equilibration of material across the surface of tubules. Variation of tubule radii found in cells could vary equilibration times by almost 50%, and we expect this factor, along with hydrodynamics (Domanov *et al.*, 2011), to also play a crucial role in setting up concentration gradients. Based on these findings, we predict that entry of membrane-bound cargo into tubes should occur most slowly in the case of slowly diffusing molecules moving into long tubes with large radii. Such a mechanism could potentially slow down the intake of cargoes to allow the cellular machinery the time to respond, for example, by scissioning the tubules and thus decoupling them from the membrane reservoir. This type of kinetic sorting model has been proposed to regulate the entry of the β2 adrenergic receptor (β2AR) into a specific class of endosomal tubules (Puthenveedu *et al.*, 2010). In that study, β2AR was shown to diffuse four times more slowly than another cargo protein, transferrin receptor, on endosomal membranes. Consequently transferrin receptor was able to enter into endosomally derived bulk recycling tubules more rapidly than β2AR could. These bulk recycling tubules scissioned from the endosomal membrane relatively rapidly, thus disfavoring the entry of β2AR. Instead, β2AR tended to accumulate in a longer-lived specialized class of endosomal tubules stabilized by actin. Interestingly, the $t_{1/2}$ for β2AR to recover on a small region of the endosomal membrane by FRAP was ~25 s. This is comparable to the lifetime of the short-lived bulk-recycling tubules (<30 s) (Puthenveedu *et al.*, 2010). Thus, even though the concentration gradients that develop across the tubules are transient, their temporal evolution ultimately has a significant biological impact on sorting.

Another prediction of our model is that, in situations in which increasing concentrations of cargo are available to flow into tubes, a concentration gradient along the length of the tube would be set up almost immediately. The geometry of tubes also dictates the temporal evolution of the shape and the magnitude of the concentration gradient along the tube surface. Such concentration gradients could play a biological role in clathrin-independent endocytosis of AB_5 toxins. These toxins not only drive the formation of tubular endocytic structures but are also known to change membrane physical properties in a concentration-dependent manner (Römer *et al.*, 2007). The cell could in principle couple the geometry of the tubule with the regulation of endocytosis to sense the cargo concentration in the tubule.

In summary, we have developed a generalizable model of diffusion in tubular geometries from fundamental diffusion equations and have simulated diffusion for various biologically relevant boundary conditions and parameters. Our findings emphasize that sorting and concentration gradients can be initiated merely by the presence of curvature in the system, without requiring that the surface-embedded molecules themselves exhibit curvature preferences. These results provide a framework for modeling diffusion in complex surfaces and suggest new numerical models for how biological functions could emerge as a consequence of the nature of diffusion in tubular geometries.

MATERIALS AND METHODS

Finite element approximations and simulation details of Laplace–Beltrami equations

We first derived a Laplace–Beltrami equation (Eq. 5 in Supplemental Text S1) for tubular surfaces. We would like to emphasize that complementary approaches for deriving the equation of continuity can be found elsewhere (Marsden *et al.*, 1984; Frankel, 2011). To solve this equation for a tubular surface, we have developed a univariate FEM solver (Oden, 2006). This FEM solver is designed for tubular diffusion under symmetric conditions, that is, all prescribed solutions are independent of the angle about the tube's center axis. Consequently the data depend only on the position along the tube's center axis. Under such symmetric conditions, the tubular diffusion has only a single degree of freedom and is modeled in a univariate setting. The symmetric tubule diffusion using defined virtual coordinates reduces to the form $u_t - k\left[A(x)u_x\right]_x = 0$ for specific forms of $A(x)$ determined by the tube's geometry. This is then solved using our 1-D FEM solver. The numerical solution is computed by semidiscrete methods. First, the uniform mesh and approximating spline space are user specified. As the basis of the symmetric solver, we use normalized B-splines $S_d^r(\Delta)$ (Schumaker, 2015). This reduces the computation time and, unlike other methods such as nodal basis elements, avoids artifacts such as negativity while smoothing the splines. We then use the De'Castlejeau algorithm for the evaluation of the B-splines without having to construct individual basis spline in the $S_d^r(\Delta)$ space. Then a Galerkin procedure is implemented. The integration is accomplished through a Gaussian quadrature exact up to polynomials of degree 11. For example, when the approximation

is conducted in any of the recommended spaces $S_2^0, S_2^1, S_3^2(\Delta)$, the quadrature is exact. The remaining temporal part is then handled using Matlab's ODE45 solver. All our simulations were performed using Matlab R2014/R2015a on Windows computers. A more general two-dimensional code capable of handling even asymmetric boundary conditions is described in Supplemental Text S2. Finally, as a note, we do remind readers that numerical approximation of this model is entirely a different problem to solve and this is independent from the model's theoretical justification and derivation. We have included ways to improve numerical solutions and avoid artifacts due to approximation in Supplemental Text S7.

Availability of the code

The complete code has been made available online at https://my.vanderbilt.edu/kenworthylab/fem-software-for-diffusion. We have also included, as a part of the code, a diffusion coefficient mapper for FRAP experiments of tubules that, given the height, radius, and $t_{1/2}$ will give out the diffusion coefficient. Instructions for use of the code are given in Supplemental Text S6.

ACKNOWLEDGMENTS

We thank Patricia Bassereau for sharing the previously published data used in Figure 5 and for providing valuable feedback. We also thank Michael Saxton for careful reading of the paper and insightful critiques. We thank Larry Schumaker for helping with the B-splines. Finally, we thank Stephen Jiminez for assisting with the numerical simulations. This work was supported by the following grants: NSF/DMS 0970008 and NSF-DMS-1265548 from the National Science Foundation and RO1 GM106720 from the National Institutes of Health. The funding sources had no role in the study design; collection, analysis, or interpretation of data; writing the report; or the decision to submit the paper for publication.

REFERENCES

Adler J, Shevchuk AI, Novak P, Korchev YE, Parmryd I (2010). Plasma membrane topography and interpretation of single-particle tracks. Nat Methods 7, 170–171.

Aimon S, Callan-Jones A, Berthaud A, Pinot M, Toombes GS, Bassereau P (2014). Membrane shape modulates transmembrane protein distribution. Dev Cell 28, 212–218.

Arroyo M, DeSimone A, Heltai L (2010). The role of membrane viscosity in the dynamics of fluid membranes. arXiv 1007.4934.

Baumgart T, Hess ST, Webb WW (2003). Imaging coexisting fluid domains in biomembrane models coupling curvature and line tension. Nature 425, 821–824.

Berk DA, Hochmuth RM (1992). Lateral mobility of integral proteins in red blood cell tethers. Biophys J 61, 9–18.

Briggman KL, Bock DD (2012). Volume electron microscopy for neuronal circuit reconstruction. Curr Opin Neurobiol 22, 154–161.

Callan-Jones A, Sorre B, Bassereau P (2011). Curvature-driven lipid sorting in biomembranes. Cold Spring Harb Perspect Biol 3, a004648.

Carlton J, Bujny M, Peter BJ, Oorschot VMJ, Rutherford A, Mellor H, Klumperman J, McMahon HT, Cullen PJ (2004). Sorting nexin-1 mediates tubular endosome-to-TGN transport through coincidence sensing of high- curvature membranes and 3-phosphoinositides. Curr Biol 14, 1791–1800.

Choquet D, Triller A (2003). The role of receptor diffusion in the organization of the postsynaptic membrane. Nat Rev Neurosci 4, 251–265.

Daniels DR, Turner MS (2007). Diffusion on membrane tubes: a highly discriminatory test of the Saffman-Delbruck theory. Langmuir 23, 6667–6670.

Daumas F, Destainville N, Millot C, Lopez A, Dean D, Salomé L (2003). Confined diffusion without fences of a G-protein-coupled receptor as revealed by single particle tracking. Biophys J 84, 356–366.

Day CA, Baetz NW, Copeland CA, Kraft LJ, Han B, Tiwari A, Drake KR, De Luca H, Chinnapen DJ, Davidson MW, *et al.* (2015). Microtubule motors power plasma membrane tubulation in clathrin-independent endocytosis. Traffic 16, 572–590.

Domanov YA, Aimon S, Toombes GES, Renner M, Quemeneur F, Triller A, Turner MS, Bassereau P (2011). Mobility in geometrically confined membranes. Proc Natl Acad Sci USA 108, 12605–12610.

Douglass AD, Vale RD (2005). Single-molecule microscopy reveals plasma membrane microdomains created by protein-protein networks that exclude or trap signaling molecules in T cells. Cell 121, 937–950.

Edwald E, Stone MB, Gray EM, Wu J, Veatch SL (2014). Oxygen depletion speeds and simplifies diffusion in HeLa cells. Biophys J 107, 1873–1884.

Eggeling C, Ringemann C, Medda R, Schwarzmann G, Sandhoff K, Polyakova S, Belov VN, Hein B, von Middendorff C, Schönle A, Hell SW (2009). Direct observation of the nanoscale dynamics of membrane lipids in a living cell. Nature 457, 1159–1162.

Eisenberg S, Shvartsman DE, Ehrlich M, Henis YI (2006). Clustering of raft-associated proteins in the external membrane leaflet modulates internal leaflet H-ras diffusion and signaling. Mol Cell Biol 26, 7190–7200.

Farsad K (2001). Generation of high curvature membranes mediated by direct endophilin bilayer interactions. J Cell Biol 155, 193–200.

Frankel T (2011). The Geometry of Physics: An Introduction, Cambridge, UK: Cambridge University Press.

Gikhman II, Skorokhod AV (1969). Introduction to the Theory of Random Processes, Philadelphia: Saunders.

Guerrier S, Coutinho-Budd J, Sassa T, Gresset A, Jordan NV, Chen K, Jin W-LL, Frost A, Polleux F (2009). The F-BAR domain of srGAP2 induces membrane protrusions required for neuronal migration and morphogenesis. Cell 138, 990–1004.

Guigas G, Weiss M (2006). Size-dependent diffusion of membrane inclusions. Biophys J 91, 2393–2398.

Harb F, Sarkis J, Ferte N, Tinland B (2012). Beyond Saffman-Delbruck approximation: a new regime for 2D diffusion of α-hemolysin complexes in supported lipid bilayer. Eur Phys J E Soft Matter 35, 1–9.

Henle ML, Levine AJ (2010). Hydrodynamics in curved membranes: the effect of geometry on particulate mobility. Phys Rev E Stat Nonlin Soft Matter Phys 81, 1–17.

Henle ML, McGorty R, Dinsmore AD, Levine AJ (2007). The effect of curvature and topology on membrane hydrodynamics. EPL (Europhys Lett) 84, 48001.

Holcman D, Schuss Z (2011). Diffusion laws in dendritic spines. J Math Neurosci 1, 10.

Jaumouillé V, Farkash Y, Jaqaman K, Das R, Lowell CA, Grinstein S (2014). Actin cytoskeleton reorganization by syk regulates fcγ receptor responsiveness by increasing its lateral mobility and clustering. Dev Cell 29, 534–546.

Jiang H, Powers TR (2008). Curvature-driven lipid sorting in a membrane tubule. Phys Rev Lett 101, 2–5.

Kenworthy AK, Nichols BJ, Remmert CL, Hendrix GM, Kumar M, Zimmerberg J, Lippincott-Schwartz J (2004). Dynamics of putative raft-associated proteins at the cell surface. J Cell Biol 165, 735–746.

Kirchhausen T (2009). Imaging endocytic clathrin structures in living cells. Trends Cell Biol 19, 596–605.

Kosmalska AJ, Casares L, Elosegui-Artola A, Thottacherry JJ, Moreno-Vicente R, González-Tarragó V, del Pozo MÁ, Mayor S, Arroyo M, Navajas D, *et al.* (2015). Physical principles of membrane remodelling during cell mechanoadaptation. Nat Commun 6, 7292.

Köster DV, Mayor S (2016). Cortical actin and the plasma membrane: inextricably intertwined. Curr Opin Cell Biol 38, 81–89.

Kozlov MM, Campelo F, Liska N, Chernomordik LV, Marrink SJ, McMahon HT (2014). Mechanisms shaping cell membranes. Curr Opin Cell Biol 29C, 53–60.

Krapf D (2015). Mechanisms underlying anomalous diffusion in the plasma membrane. Curr Top Membr 75, 167–207.

Kusters R, Kapitein LC, Hoogenraad CC, Storm C (2013). Shape-induced asymmetric diffusion in dendritic spines allows efficient synaptic AMPA receptor trapping. Biophys J 105, 2743–2750.

Kusters R, Paquay S, Storm C (2014). Confinement without boundaries: anisotropic diffusion on the surface of a cylinder. arXiv 1407.3564.

Kusters R, Storm C (2014). Impact of morphology on diffusive dynamics on curved surfaces. Phys Rev E Stat Nonlin Soft Matter Phys 89, 032723.

Kusumi A, Ike H, Nakada C, Murase K, Fujiwara T (2005). Single-molecule tracking of membrane molecules: plasma membrane compartmentalization and dynamic assembly of raft-philic signaling molecules. Semin Immunol 17, 3–21.

Kusumi A, Shirai YM, Koyama-Honda I, Suzuki KGN, Fujiwara TK (2010). Hierarchical organization of the plasma membrane: investigations by single-molecule tracking vs. fluorescence correlation spectroscopy. FEBS Lett 584, 1814–1823.

Lajoie P, Partridge EA, Guay G, Goetz JG, Pawling J, Lagana A, Bharat J, Dennis JW, Nabi IR (2007). Plasma membrane domain organization regulates EGFR signaling in tumor cells. J Cell Biol 179, 341–356.
Larsen JB, Jensen MB, Bhatia VK, Pedersen SL, Bjørnholm T, Iversen L, Uline M, Szleifer I, Jensen KJ, Hatzakis NS, Stamou D (2015). Membrane curvature enables N-Ras lipid anchor sorting to liquid-ordered membrane phases. Nat Chem Biol 11, 192–194.
Leitenberger SM, Reister-Gottfried E, Seifert U (2008). Curvature-coupling dependence of membrane protein diffusion coefficients. Langmuir 24, 1254–1261.
Marsden JE, Hughes TJR, Carlson DE (1984). Mathematical Foundations of Elasticity, New York: Dover Publications.
McMahon HT, Boucrot E (2015). Membrane curvature at a glance. J Cell Sci 128, 1065–1070.
Mogilner A, Rubinstein B (2005). The physics of filopodial protrusion. Biophys J 89, 782–795.
Mukherjee S, Maxfield FR (2000). Role of membrane organization and membrane domains in endocytic lipid trafficking. Traffic 1, 203–211.
Mukherjee S, Maxfield FR (2004). Membrane domains. Annu Rev Cell Dev Biol 20, 839–866.
Oden JT (2006). Finite Elements of Nonlinear Continua, New York: Dover Publications.
Pazour GJ, Witman GB (2002). The vertebrate primary cilium is a sensory organelle. Curr Opin Cell Biol 15, 105–110.
Petrov EP, Schwille P (2008). Translational diffusion in lipid membranes beyond the Saffman-Delbruck approximation. Biophys J 94, L41–L43.
Puthenveedu MA, Lauffer B, Temkin P, Vistein R, Carlton P, Thorn K, Taunton J, Weiner OD, Parton RG, von Zastrow M (2010). Sequence-dependent sorting of recycling proteins by actin- stabilized endosomal microdomains. Cell 143, 761–773.
Rahimi M, Arroyo M (2012). Shape dynamics, lipid hydrodynamics, and the complex viscoelasticty of bilayer membranes. Phys Rev E Stat Nonlin Soft Matter Phys 86, 1–15.
Rahimi M, DeSimone A, Arroyo M (2013). Curved fluid membranes behave laterally as effective viscoelastic media. Soft Matter 9, 11033.
Ramesh P, Baroji YF, Reihani SNS, Stamou D, Oddershede LB, Bendix PM (2013). FBAR syndapin 1 recognizes and stabilizes highly curved tubular membranes in a concentration dependent manner. Sci Rep 3, 1565.
Rao Y, Haucke V (2011). Membrane shaping by the Bin/amphiphysin/Rvs (BAR) domain protein superfamily. Cell Mol Life Sci 68, 3983–3993.
Renard H-F, Simunovic M, Lemière J, Boucrot E, Garcia-Castillo MD, Arumugam S, Chambon V, Lamaze C, Wunder C, Kenworthy AK, *et al*. (2015). Endophilin-A2 functions in membrane scission in clathrin-independent endocytosis. Nature 517, 493–496.
Renner M, Domanov Y, Sandrin F, Izeddin I, Bassereau P, Triller A (2011). Lateral diffusion on tubular membranes: quantification of measurements bias. PLoS One 6, e25731.
Römer W, Berland L, Chambon V, Gaus K, Windschiegl B, Tenza D, Aly MR, Fraisier V, Florent JC, Perrais D, *et al*. (2007). Shiga toxin induces tubular membrane invaginations for its uptake into cells. Nature 450, 670–675.
Roux A, Cuvelier D, Nassoy P, Prost J, Bassereau P, Goud B (2005). Role of curvature and phase transition in lipid sorting and fission of membrane tubules. EMBO J 24, 1537–1545.
Saffman PG, Delbruck M, Delbrück M (1975). Brownian motion in biological membranes. Proc Natl Acad Sci USA 72, 3111–3113.
Sbalzarini IF, Mezzacasa A, Helenius A, Koumoutsakos P (2005). Effects of organelle shape on fluorescence recovery after photobleaching. Biophys J 89, 1482–1492.
Schumaker LL (2015). Spline Functions: Computational Methods, Nashville, TN: SIAM.
Scorrano L, Ashiya M, Buttle K, Weiler S, Oakes SA, Mannella CA, Korsmeyer SJ (2002). A distinct pathway remodels mitochondrial cristae and mobilizes cytochrome *c* during apoptosis. Dev Cell 2, 55–67.
Simunovic M, Voth GA, Callan-Jones A, Bassereau P (2015). When physics takes over: BAR proteins and membrane curvature. Trends Cell Biol 25, 1–13.
Singh P, Mahata P, Baumgart T, Das SL (2012). Curvature sorting of proteins on a cylindrical lipid membrane tether connected to a reservoir. Phys Rev E Stat Nonlin Soft Matter Phys 85, 1–10.
Sorra KE, Harris KM (2000). Overview on the structure, composition, function, development, and plasticity of hippocampal dendritic spines. Hippocampus 10, 501–511.
Suetsugu S, Gautreau A (2012). Synergistic BAR-NPF interactions in actin-driven membrane remodeling. Trends Cell Biol 22, 141–150.
Tian A, Baumgart T (2009). Sorting of lipids and proteins in membrane curvature gradients. Biophys J 96, 2676–2688.
Treanor B, Depoil D, Gonzalez-Granja A, Barral P, Weber M, Dushek O, Bruckbauer A, Batista FD (2010). The membrane skeleton controls diffusion dynamics and signaling through the B cell receptor. Immunity 32, 187–199.
Trimble WS, Grinstein S (2015). Barriers to the free diffusion of proteins and lipids in the plasma membrane. J Cell Biol 208, 259–271.
Upadhyaya A, Sheetz MP (2004). Tension in tubulovesicular networks of Golgi and endoplasmic reticulum membranes. Biophys J 86, 2923–2928.
Wang Q, Navarro MVAS, Peng G, Molinelli E, Goh SL, Judson BL, Rajashankar KR, Sondermann H (2009). Molecular mechanism of membrane constriction and tubulation mediated by the F-BAR protein Pacsin/Syndapin. Proc Natl Acad Sci USA 106, 12700–12705.
Waterman-Storer CM, Salmon ED (1998). Endoplasmic reticulum membrane tubules are distributed by microtubules in living cells using three distinct mechanisms. Curr Biol 8, 798–806.
Westermann M, Leutbecher H, Meyer H (1999). Membrane structure of caveolae and isolated caveolin-rich vesicles. Histochem Cell Biol 111, 71–81.
Windebank AJ, Wood P, Bunge RP, Dyck PJ (1985). Myelination determines the caliber of dorsal root ganglion neurons in culture. J Neurosci 5, 1563–1569.
Wu Q-Y, Liang Q (2014). Interplay between curvature and lateral organization of lipids and peptides/proteins in model membranes. Langmuir 30, 1116–1122.
Yoshigaki T (2007). Theoretically predicted effects of Gaussian curvature on lateral diffusion of membrane molecules. Phys Rev E Stat Nonlin Soft Matter Phys 75, 1–16.
Zhu C, Das SL, Baumgart T (2012). Nonlinear sorting, curvature generation, and crowding of endophilin N-BAR on tubular membranes. Biophys J 102, 1837–1845.
Zimmerberg J, Kozlov MM (2006). How proteins produce cellular membrane curvature. Nat Rev Mol Cell Biol 7, 9–19.